

Employing polyhedral methods to optimize stencils on FPGAs with stencil-specific caches, data reuse, and wide data bursts

Florian Mayer, Julian Brandner, and Michael Philippsen
{florian.andrefranc.mayer,julian.brandner,michael.philippsen}@fau.de

Programming Systems Group, Friedrich-Alexander Universität Erlangen-Nürnberg (FAU), Germany

Abstract

It is well known that to accelerate stencil codes on CPUs or GPUs and to exploit hardware caches and their lines optimizers must find spatial and temporal locality of array accesses to harvest data-reuse opportunities. On FPGAs there is the burden that there are no built-in caches (or only pre-built hardware descriptions for cache blocks that are inefficient for stencil codes). But this paper demonstrates that this lack is also a chance as polyhedral methods can be used to generate stencil-specific cache-structures of the right sizes on the FPGA and to fill and flush them efficiently with wide bursts during stencil execution. The paper shows how to derive the appropriate directives and code restructurings from stencil codes so that the FPGA compiler generates fast stencil hardware. Switching on our optimization improves the runtime of a set of 10 stencils by between 43× and 156×.

1 Introduction

In mature polyhedral compilers, loop tiling is a common optimization when targeting CPUs or GPUs. It restructures a loop such that it processes the iteration space block-by-block and it constructs tiles that access most of the array elements often and in the same order in which they reside in memory, i.e., with temporal and spatial locality.

There have been attempts to offload codes to FPGAs, i.e., to use a hardware synthesis (HLS) to generate circuits for them on the FPGA. However, out of the box tiled loops [12, 30] in general do not turn into efficient FPGA circuits. There are two main obstacles. First, the HLS cannot turn the tiled loop into hardware pipelines (as the loop boundaries and increments are too complex for the HLS to detect patterns). Without hardware pipelining the benefits of FPGA accelerators vanish. Second, on CPUs or GPUs tiled loops run faster since their data locality exploits the built-in cache hierarchy. As on FPGAs there are no caches, there is no benefit from tiling alone. In general, the HLS generates from the tiled loop a hardware block (kernel) with connections to an FPGA bus through which the kernel directly talks to the DDR, i.e., without any host-side cache support. There are two approaches

to still allow loop tiles to enjoy data locality. One can either add an FPGA hardware block that implements a cache between the kernel and the DDR. FPGA hardware vendors offer such pre-fabricated hardware descriptions. Such cache circuits on the FPGA have been used to accelerate FPGA kernels [6]. Similar to host-side cache hardware they only come with a few different sizes and they only can load lines of adjacent data and predict what to best replace. But if cache circuits need to be added to the FPGA anyway one can do better than using a generic cache block. For stencil codes this paper shows that by using polyhedral methods to understand the access patterns we can statically determine (a) the stencil-specific best cache sizes and (b) pre-load exactly what is needed and spill what is no longer needed. But the polyhedral method can also (c) help improve the burst behavior. While off-the-shelf caches have a fixed line size on the side to the DDR and a fixed word size on the side to the running code, a better memory bandwidth can be reached with wide (and stencil-specific) bursts. We show how to use polyhedral methods to achieve the data alignment requirements. Even more, instead of asking the HLS to construct such a stencil-specific cache and add it between kernel and DDR, we (d) inline the cache functionality, i.e., we use buffer arrays and load operations within the stencil.

The main contribution of this work is a polyhedral-based code generator for FPGAs. It uses loop tiling to improve locality, adds buffers and directives to generate inlined cache-like hardware circuits that exploit that locality, and calculates a data-shipment that uses wide bursts to fill these caches.

Sec. 2 introduces our loop tiling terminology. Sec. 3 covers our cache buffers, their types, and their fusion. Both sections set the stage for explaining our optimization in Sec. 4. Sec. 5 reviews related work before we present our quantitative results in Sec. 6 and conclude.

2 Notation for Tiling Transformations

An optimizing compiler tiles a loop by cutting its iteration space into segments of size SZ , so-called tiles. The result is an outer loop (inter-tile loop, index ti) that holds an inner loop (intra-tile loop, original index i , original body). In Fig. 1 we tile the given loop with a tile size of $SZ = 32$. Since the original iteration space may not be divisible by SZ the first and/or the last tiles in general have fewer than SZ iterations.

```

// Original loop
for (i=1; i<N; i+=1)
    A[i] = B[i-1] + B[i+1];

// Tiling 1: with SZ=32 (here Δ=0)
// iterations per tile: 32, 32*, rest
for (ti=1; ti<N; ti+=32)
    for (i=max(1, ti); i<min(N, ti+32); i+=1)
        A[i] = B[i-1] + B[i+1];

// Tiling 2: with SZ=32 and Δ=1
// iterations per tile: 32-1=31, 32*, rest
for (ti=1; ti<N; ti+=32)
    for (i=max(1+1, ti); i<min(N-1, ti+32); i+=1)
        A[i-1] = B[i-1-1] + B[i+1-1];

// Tiling 3: with SZ=32 (normal form, δ=(0,0))
// iterations per tile: 31, 32*, rest
for (ti=0; ti<N; ti+=32)
    for (i=max(1, ti); i<min(N-1, ti+31); i+=1)
        A[i] = B[i-1] + B[i+1];

// Tiling 4: with SZ=32 and δ=(-1,0)
// iterations per tile: 32, 32*, rest
for (ti=1; ti<N; ti+=32)
    for (i=ti; i<min(N-1, ti+31); i+=1)
        A[i] = B[i-1] + B[i+1];

// Tiling 5: with SZ=32 and δ=(-1,-ti)
// iterations per tile: 32, 32*, rest
for (ti=1; ti<N; ti+=32)
    for (i=0; i<min(31, N-ti-1); i+=1)
        A[i+ti] = B[i-1+ti] + B[i+1+ti];

// Tiling 6: with SZ=32 and δ=(-1,-ti), padded
// iterations per tile: 32, 32*, rest
for (ti=1; ti<N; ti+=32)
    for (i=0; i<=31; i+=1)
        A[i+ti] = B[i-1+ti] + B[i+1+ti];

```

Figure 1. Loop Tiling Example.

On CPUs/GPUs the purpose of tiling is to enhance cache locality. When the code accesses a memory address, the built-in cache hardware loads a full line that also includes adjacent addresses. In the ideal case, the tile size fits to the size of the cache lines and when a tile loop accesses an address in its first iteration, the cache hardware pre-loads all the data that later iterations of the tile need for faster accesses without cache-misses. However, this effect is only visible if the boundaries of the tiles are properly aligned w.r.t. the addressing requirements of the cache hardware. Hence, in addition to picking a tile size, the optimizing compiler also picks a Δ that (slightly) shifts the boundaries of the tile loops, i.e., the first tile starts Δ iterations later and is shorter by Δ iterations. The inner tiles keep their sizes. The last tile grows by Δ iterations. In Fig. 1 the Tiling 1 does not have such a shift ($\Delta = 0$). The second one uses $\Delta = 1$. Such a shifting of the tile boundaries is important when targeting an architecture with built-in cache hardware. However, when targeting an FPGA, it is necessary to generalize the concept of shifting to both the outer and the inner loop. This turns Δ into a vector $\delta = (\delta^o, \delta^i)$. For a simpler formalism, we also calibrate the outer loop to start from 0 as shown in Tiling 3. We call this

the normal form, $\delta = (0, 0)$. Unfortunately, the HLS cannot generate an efficient FPGA from the normal form. Only if its analysis can prove that the loop boundaries are runtime constants, the HLS unrolls a loop into parallel/pipelined circuits. The max and min operations in the boundaries of the inner tile loop hide from the HLS that this is the case. By shifting the outer loop by $\delta^o = -1$ its first index value matches the starting index of the original loop (and this also ensures that the first tile is a full tile of size SZ). The more important effect is that the max operation is no longer needed, as Tiling 4 shows. But the HLS still does not understand the lower bound expression $i=ti$ of the inner loop. Only by shifting the inner loop by $\delta^i = -ti$ so that it starts from a constant 0, we can make the HLS generate unrolled and parallel circuits for it. Note, that because of the normalization for any vector δ , i.e., for the last three tilings, the following predicate holds for the loop indices:

$$(ti + \delta^o) \bmod SZ = 0 \wedge ti \leq i < ti + SZ$$

In addition, some compilers also pick an execution order o for the iterations of a tile, e.g., to run a loop backwards. Formally, the bijective ordering function o maps an index i of the tile loop to an $o(i)$. The lexicographic order of the values $o(i)$ is the execution order of the tile. While for any choices of SZ and δ a tiling is always valid, altering the order o may break the data dependences that exist in the original loop. This paper does not take reordering into account.

Loop tiling can recursively be applied to each of the loops in a given loop nest of depth d . To achieve the intended effects on locality of accesses, compilers in general first re-group the resulting $2d$ loops and interchange them so that all the d inter-tile loops surround all the d intra-tile loops. They then pick a permutation p of size d that shuffles/interchanges the d inner (tile) loops to select the tiling with best locality. Re-grouping and interchanging the loops in a loop nest may break data dependences that exists in the original loop nest.

The take-away is, that when ignoring iteration space re-orderings and taking the initial re-grouping into inter-tile loops followed by intra-tile loops as given, a *tiling transformation* T for a d -dimensional loop nest is fully specified by a triple (SZ, p, δ) with a vector of tile sizes $SZ=(SZ_1, \dots, SZ_d)$, a permutation p indicating how to shuffle the intra-tile loops, and a delta vector $\delta = (\delta_1^o, \delta_1^i, \dots, \delta_d^o, \delta_d^i)$. Formally, for the indices of the resulting $2d$ loops the effect of T is:

$$T(SZ, p, \delta) = \{O[i_1, \dots, i_d] \rightarrow$$

$$O[ti_1, \dots, ti_d, p(i_1) + \delta_{p(i_1)}^i, \dots, p(i_d) + \delta_{p(i_d)}^i] :$$

$$\bigwedge_{x=1}^d (ti_x + \delta_x^o) \bmod SZ_x = 0 \wedge ti_x \leq i_x < ti_x + SZ_x\}$$

Note, that the lexicographical order $O[i_1, \dots, i_d]$ in which the d original loops are executed is replaced by a $2d$ -dimensional order for the resulting loop nest of depth $2d$.

The polyhedral toolbox [3–5, 10, 11, 16] is a set of operators and functions that help work with tiling transformations (and other loop optimizations). To do so, the toolbox relies

```

for (i=1; i<N-1, i++)
  for (j=1; j<N-1; j++)
    for (k=1; k<N-1; k++)
      S:  V[i,k,j] = V[i,k,j] + A[i,j,k]
          + A[i+1,j+1,k+1];

```

SCoP of the above loop nest:

$$\begin{aligned}
Dom &= [N] \rightarrow \{S[i, j, k] : \\
&\quad 1 \leq i < N - 1 \wedge 1 \leq j < N - 1 \wedge 1 \leq k < N - 1\} \\
Sch &= \{S[i, j, k] \rightarrow O[i, j, k]\} \\
R_0 &= \{S[i, j, k] \rightarrow V[i, k, j]\} \\
R_1 &= \{S[i, j, k] \rightarrow A[i, j, k]\} \\
R_2 &= \{S[i, j, k] \rightarrow A[i+1, j+1, k+1]\} \\
W_0 &= \{S[i, j, k] \rightarrow V[i, k, j]\}
\end{aligned}$$
Figure 2. Running Example.

```

// outer loops, inter-tile
for (ti=0; ti < N-1; ti += SZ_i)
  for (tj=0; ...)
    for (tk=0; ...)
      // inner loops, intra-tile, p=(i,k,j)
      for (i=max(...); i<=min(...); i++)
        for (k=max(...); ...)
          for (j=max(...); ...)
            S(i, j, k);

```

Modified parts of the SCoP:

$$\begin{aligned}
Sch' &= \{S[i, j, k] \rightarrow O[t_i, t_j, t_k, i, k, j] : \\
&\quad t_i \bmod SZ_i = 0 \wedge t_i \leq i < t_i + SZ_i \wedge \dots \\
&\quad t_k \bmod SZ_k = 0 \wedge t_k \leq k < t_k + SZ_k\}
\end{aligned}$$
Figure 3. Normal form of tiling the code in Fig. 2 with the transformation $T(SZ = (SZ_i, SZ_j, SZ_k), p = (i, k, j), \delta = (0, 0, 0, 0, 0, 0))$. S is a shorthand of the original loop body.

on some formalism describing loop nests, the data accesses in their bodies, and the index sets involved (today often encoded with the Integer Set Library (ISL) [30]). The key element of the formalism is a so-called Static Control Part (SCoP) that represents a loop nest. It consists of the domain set Dom that models the iteration space of the loop nest, a schedule Sch that defines the order of iterations by mapping iterations to a lexicographic order O , and a list of access relations for reading R and writing W . They represent the array accesses of the individual iterations. A loop nest can be represented with a SCoP if in its code all conditions and loop bounds are affine functions of runtime constants and loop indices. In this paper we require all array accesses to also be in that form. Fig. 2 holds a $d = 3$ dimensional running example and its SCoP. The schedule Sch maps the iteration vector (i, j, k) to the lexicographic order. When handed this SCoP, the polyhedral toolbox can detect that R_0 and W_0 address the same data element in every iteration (i, j, k) . Fig. 3 is the result of applying a tiling transformation. In the resulting SCoP, only Sch changes. Sch' turns the execution order into a 6-dimensional lexicographic one and it restricts the index values as defined by $T(SZ, p, \delta)$ above.

3 Cache buffers: Types and Fusion

Cache Buffers for Working Sets of Tiles. Assume a stencil had only one single array access. The fundamental idea of our approach is to use a stencil-specific cache buffer that holds all the data elements that a single tile needs, i.e., that – for a fixed set of loop indices of the d outer loops – all iterations of the d inner loops of a tiling access. We call these data elements the *working set* of a tile. Such a cache can improve the total runtime of a tile because of two reasons: First, it may be possible to apply an efficient burst load to fill the cache (spatial locality) before the tile starts its execution and to then serve the tile with faster accesses to the cached data instead of accesses to the copies residing in the DDR and, second, to benefit even more if the tile accesses cached data elements more than once (temporal locality). For general n -point stencils we aim to use one buffer per array access.

For the single access to a d -dimensional array A , a tile with sizes $SZ = (SZ_1, \dots, SZ_d)$ has a working set of $\prod_1^d SZ_i$ data elements (for many types of stencils) that can be stored in a d -dimensional buffer array of size $\prod_1^d SZ_i$. We call this a *full buffer* (of A in a tiling). If the running example only had the access to $A[i+1, j+1, k+1]$ then a buffer array of size 32^3 could be filled before the start of a tile's execution so that the tile could work with the data in that buffer. Whereas for the stencil of the running example, the tile sizes suffice to compute the size of the buffer array, in general, it is necessary to calculate the minimal *bounding box* around the data elements in the working set.¹ For example, if instead of $j+1$ the second index is $2*j$, we would need a buffer twice as large to hold all the accessed array elements (plus the unused ones between them). Only if the size of the bounding box is statically known, a buffer array can be used for caching. Otherwise we label the array access as **nc** (no caching).

There are ways to use smaller caches/buffers without losing the advantages of pre-loading. Instead of pre-loading the full working set of a tile, we look at the sub-tiles that the outermost intra-tile loop processes. Such a sub-tile has the same d -dimensional array access in its body and hence, in general, it needs the same full buffer to store its working set. But for a fixed index of the outermost tile loop, the bounding boxes of the array accesses often are much smaller than the tile sizes. In this case, we pre-load only those elements into

¹From the working set $ws = A(f)$ for an access relation A and a set of iterations of a full tile $f = [t_{i_1}, \dots, t_{i_d}] \rightarrow \{O[t_{i_1}, \dots, t_{i_d}, i_{p(i_1)}, \dots, i_{p(i_d)}]\}$ we project out the d dimensions $dims = proj(ws)$ by means of $proj = \{[i_1, \dots, i_d] \rightarrow A_{i_1}[i_1]; \dots; [i_0, \dots, i_d] \rightarrow A_{i_d}[i_d]\}$. The corners of the bounding box are the lexicographically smallest ($lmins = lmin(dims)$) or largest ($lmaxs = lmax(dims)$) index values per dimension. To calculate the extent of the bounding box, we build a set per dimension that contains all elements between the smallest and the largest element. Thus, for each universe set u in $S(univ(dims))$, where S is the space decomposition operator, we build the one-dimensional interval set in by $lb(lmin) \cap ub(lmax)$, where $lb = (lmins \cap u) \leq univ(lmins \cap u)$ and $ub = (lmaxs \cap u) \geq univ(lmaxs \cap u)$. The intersection of the inverse projections of the d interval sets, $\bigcap_{i=1}^d proj^{-1}(in_i)$, is the bounding box of ws .

the smaller cache (ideally with a burst load) before a sub-tile starts. We call such a buffer a *chunk* buffer. In the running example for a fixed value of i (the index of the outermost tile loop), the bounding box of the working set has a width of 1 in the i -dimension. Thus all the elements that the sub-tile accesses only need a much smaller buffer of size $1 \cdot 32 \cdot 32$.

Chunk buffers need fewer FPGA resources than full buffers, leave more FPGA floor space for the tiles' circuits, and allow larger tiles with more parallelism. But there is a downside. As long as there is a pre-loading phase followed by a tile's execution phase and a write-back phase that is needed in case of write accesses, in general there is a runtime penalty due to redundant data loadings. Consider a chunk of data that the outermost tile loop loads into the chunk buffer. Whenever the loop ticks, most of the data elements in the buffer are likely to be loaded again, albeit into a separate slice of the buffer array. While the chunk buffer is smaller than the full buffer, the runtime performance in general drops due to the redundant loadings. The chunk buffer is only a wise choice for tiling permutations that allow to shift the data locally within the buffer instead of reloading it from the DDR. Then a chunk buffer can be used even more efficiently by partly overlapping the pre-loading and the sub-tile's execution. Instead of pre-loading all its elements, it is possible to pre-load only the data elements that the first few iterations of the sub-tile need. And while those iterations are busy, the FPGA-circuits *concurrently* pre-load only what the next iteration of the sub-tile will need. Whenever a sub-tile iteration is done, the data in the chunk buffer shifts along its outermost axis. Note that it depends on the tiling permutations whether a chunk buffer is useful. It can be applied if each sub-tile needs a data chunk of the same size and if the data shift between any two adjacent sub-tiles only depends on the index of the outermost tile loop. For the permutation $p = (i, k, j)$ of the running example we cannot use a chunk buffer for the access $A[i+1][j+1][k+1]$ as p does not permit data bursts to fill it. Only for $p = (., ., k)$ we can pick a chunk buffer for A .

For the chunk buffer we kept the index of the outermost intra-tile loop fixed. A generalization is to fix the index values of all but the innermost intra-tile loops, i.e., to only look at its working set, that, as before, often can be stored in a smaller cache buffer. There is a special case with an even smaller FPGA footprint and more concurrent pre-loading: If for the array access the sizes of the working set bounding boxes are 1 in all but one of its dimensions, then a one-dimensional array can be used as a so-called *line* buffer. In the running example, assume fixed values for i and k , then for $A[i+1][j+1][k+1]$ the size of the one-dimensional buffer array is $1 \cdot 32 \cdot 1$. Similar to the situation with chunk buffers, conceptually all tiling permutations could use a line buffer, but only some of them allow for a pre-loading with data bursts while others require a much slower initialization of the complete line. For the running example we cannot pick a line buffer, as the access to A is not in line w.r.t. the inner j loop (and thus slow).

Fusion of Caches for Temporal Locality. Now that we have discussed how to achieve spatial locality with smaller cache buffers and how the best choice depends on the tiling permutation, let us improve the general idea to n -point stencils that have more than one array access and that may have data dependences among their accesses. We aim to exploit the data reuse potential and save on the number and total sizes of the cache buffers needed for such stencils.

If a stencil has two accesses to the same array (both without **nc**-label), there are two cases that matter: (a) One can use a combined cache buffer for both of them if the size of the combined cache buffer is smaller than the sum of the sizes of the two individual cache buffers. (b) It may not be possible to use a cache buffer for any of the accesses if there is a (loop carried) data dependence.

To check if a case applies, we use the polyhedral toolbox to compute the intersection of the working sets of the two array accesses.² For an *empty* intersection (not shown in the running example) we use separate cache buffers and pick their types as discussed above. For a *non-empty* intersection there are two cases. If there is no data dependence between the two accesses, we *can* use a shared cache, fuse their working sets, and pick the buffer type that fits the union of the sets. We only fuse if this reduces the total memory demands and if it does not turn the fused accesses into **nc** ones. For example, there may be array accesses that, individually, have working sets suitable for small chunk (or even line) buffers. But the union of their working sets may need a full buffer or – even worse – may not be suitable for caching at all due to a statically unknown size. If there is a data dependence, we either *must* use a shared cache for both working sets or refrain from using caches at all. Separate caches may break the data dependence, as a value written into one cache may not be observed by a read from the other cache. We label both array accesses as **nc** and do not use a cache buffer for them at all. In general, there can be a set of accesses (not just two) that form a graph of data dependences. We label all those accesses as **nc** as soon as there is an empty intersection of the working sets of any pair of accesses in that set. (This is a simplification: there may be some pairs in the set that could use a shared cache buffer without breaking the data dependence. This paper ignores the optimization potential.)

In the running example the two accesses to A have a non-empty intersection. The same holds for both accesses to V . On its left side, Fig. 4 shows the fused accesses. We apply the selection process discussed above to pick the suitable

²Consider one of the array accesses, say $A[i, j, k]$ which is R_1 in the SCoP. To compute its working set, the term $R'_1 = (R_1^{-1} \cdot Sch')^{-1}$ turns the original access relation R_1 in the given SCoP into R'_1 that reflects the schedule Sch' after tiling and maps $O[ti_1, \dots, ti_d, i_1, \dots, i_d] \rightarrow A[i_1, \dots, i_d]$. Once we have pre-processed the two access relations that way, we can apply the set of all iterations in a full tile ($full = [ti_1, \dots, ti_d] \rightarrow \{O[ti_1, \dots, ti_d, i_{p(i_1)}, \dots, i_{p(i_d)}]\}$) to both of them and compute the intersection $R'_1(full) \cap R'_2(full)$. (Same for W access relations.)

	$p = (i, k, j)$	$p = (i, j, k)$
<div style="border: 1px solid black; padding: 5px; display: inline-block;"> $A[i, j, k],$ $A[i + 1, j + 1, k + 1]$ </div>	full buffer $A' = [33, 33, 33]$	chunk buffer $A' = [2, 33, 33]$
<div style="border: 1px solid black; padding: 5px; display: inline-block;"> $V[i, k, j],$ $V[i, k, j]$ </div>	chunk buffer $V' = [1, 32, 32]$	full buffer $V' = [32, 32, 32]$
total cost:	$33^3 + 1 \cdot 32^2 = 36\,961$	$2 \cdot 33^2 + 32^3 = 34\,946$

Figure 4. Fused working sets and selected cache buffers (types and sizes) for two out of six feasible permutations for the running example with tile sizes $SZ = (32, 32, 32)$.

cache buffer types for them and to gauge their sizes (and thus implicitly their potential for concurrent pre-loading). Recall that this choice depends on the permutation. If the shared buffer does not save space we keep the buffers separate.

The two working sets of two array accesses of A are different from the union of those sets. The tile accesses in each of the array dimensions an element plus its adjacent element. The sizes of the bounding boxes of the combined working set are thus $[33, 33, 33]$ instead of $[32, 32, 32]$ for both of the individual accesses. Let us first consider the permutation $p = (i, k, j)$ that the running example uses. Here the decision process described above cannot pick chunk buffers (as p 's last index isn't k) and thus picks *two* full buffers of size 32^3 for the individual accesses. For the combined working set it picks *one* full buffer A' of size 33^3 . Since this is smaller, we fuse and use a shared buffer, see the middle column of Fig. 4.

If the running example had used a different permutation $p = (i, j, k)$ there would be chunk buffers for both individual A accesses, each with size $1 \cdot 32 \cdot 32$. The size of the bounding box of the i -dimension of the combined working set is 2 because the tile accesses both $A[i][\cdot][\cdot]$ and $A[i+1][\cdot][\cdot]$. One chunk buffer A' of size $2 \cdot 33 \cdot 33$ is better than two chunk buffers of size $1 \cdot 32 \cdot 32$. In its last column, Fig. 4 shows this choice. (Rationale: The innermost loop index k allows fast pre-loading from A' , the working sets of each sub-tile for fixed i all have the same sizes, and their data chunks can be shifted with a constant offset to avoid re-reads.) At first glance, the savings do not seem to be large. However, as discussed before, the data can now quickly be shifted locally within the fused buffer instead of reloading the same data slowly from the DDR (per tick of the outermost tile loop).

For the two accesses to V in the running example the union of their working sets is identical to the individual working sets. In case of the permutation $p = (i, k, j)$ we save by using one full buffer for it. For $p = (i, j, k)$ even a chunk buffer can be used, see Fig. 4 for the sizes.

A comparison of the two permutation columns of Fig. 4 reveals that their total costs, i.e., the sums of the sizes of the necessary cache buffers are different. Selecting the cheaper permutation $p = (i, j, k)$ not only leaves more FPGA floor space for larger tile sizes and hence more parallelism. But

smaller buffers also allow for faster and even concurrent pre-loading, without losing their ability to exploit data reuse.

4 Optimization Method

Our optimization can process n -point stencils that live in a canonical loop nest with a rectangular iteration domain, that can be represented by a SCoP, and that work on non-overlapping m -dimensional rectangular arrays with arbitrarily many reads or writes. Except for the array accesses there may not be statements with other observable side effects (although we allow for floating point divisions by zero). Our optimization works on in-place stencils, but excludes those where tiling breaks the data dependences of the stencil (e.g. Gauss-Seidel or SOR methods).

Our optimization works in five steps. Step 1 picks the tiling sizes SZ . Step 2 selects a permutation p of the inner tile loops and also assigns possibly shared cache buffers to the accesses. Step 3 chooses the deltas δ that shift tile boundaries for better HLS generated hardware. Step 4 redirects the indexing expressions from the original array to instead address the assigned cache buffers. Step 5 generates loop code, inserts buffer declarations, suitable HLS directives, and data shipment. Below we discuss these steps in detail and illustrate them with the running example in Fig. 2.

Step 1 – Picking the tile sizes SZ Whereas for CPUs or GPUs with built-in cache hardware, the tile sizes need to fit the fixed line size of the cache, conceptually we can pick any tile sizes when offloading stencils plus stencil-specific cache functionality to an FPGA. As larger tiles in general cause more parallelism by unrolling plus pipelining and thus run faster, we aim at the largest possible tile sizes that the FPGA floor can hold. However, since larger tiles need larger caches that compete for the floor space, the combined resource consumption limits the possible tile sizes. In an ideal world, an autotuner [2] can find the best configuration.

In the real world there is another limit. It is the time that the high-level synthesis takes to generate the specification of the FPGA circuits. This time strongly grows with the tile sizes (and the parallelism that they cause). We found that when allowing 3-5 hours to perform the HLS for a stencil code in our benchmark set (see Sec. 6), the largest practical tile sizes for our benchmarks are $SZ=(1024)$ for $d=1$ stencils, $SZ=(128, 128)$ for $d=2$, and $SZ=(32, 32, 32)$ for $d=3$ codes.

Step 2 – Picking a tiling permutation with the smallest cache buffers We generate the set of all feasible permutations p of the inner tile loops and purge those that violate data dependences. For each remaining permutation, we assign caches to the array accesses as described in Sec. 3, i.e., we pick a buffer type for an array access or decide that it cannot be cached (either because the size of its boundary box is not statically known or because there are data dependences that forbid caching), and whenever possible, we fuse

accesses to save space with their shared buffers. We then calculate the total size of all assigned buffers and pick the permutation with the lowest cache demand (smallest total cost). When there is a tie, we pick the permutation that uses faster buffers (*line* faster than *chunk*, *chunk* faster than *full*).

For the running example all 6 feasible permutations are valid as the stencil does not have any loop carried dependences. Sec. 3 does not assign the **nc**-flag to any of the accesses. For two of the permutations we discussed the total cost above. As the other 4 permutations are not cheaper, we pick (i, j, k) and the buffer assignment shown in Fig. 4.

Step 3 – Picking a delta and an iteration padding Consider Fig. 1 again. When the HLS generates FPGA circuits from the code of Tiling 3, there is no concurrency – the FPGA processes the iterations sequentially. The HLS cannot unroll/pipeline the tile loop in a way that builds concurrent circuits for its iterations. Current HLS tools can only unroll/pipeline loops whose bodies have statically known sizes (when unrolled recursively). In particular the obstacles are that the *max*- and the *min*-expressions used for the bounds of the inner tile loop are too complex for the pattern matching of the HLS, and that the tile loop starts from a symbolic *ti* that the HLS does not identify as being runtime constant. Step 3 picks a delta vector that gets rid of these obstacles.

Fig. 1 shows in Tiling 4 the effect of $\delta = (-1, \cdot)$. By setting δ^0 to the negated lower bound of the original untiled loop we get rid of the *max*-operation, extend the first tile to a full tile, and have an inner tile loop that starts from $i = ti$. We apply this δ^0 -shift to all loops of a given SCoP by using polyhedral operations³ that affect the schedule *Sch* of the loop nest, see the δ^0 terms in the $T(SZ, p, \delta)$ -formula in Sec. 2.

The delta $\delta = (\cdot, -ti)$ in Fig. 1 causes the inner tile loop to start from a constant 0 (Tiling 5). By setting $\delta^i = -ti$ we get rid of the symbolic *ti* and shift the inner tile loop by an offset of *ti* to then start from $i = 0$. We also apply this δ^i -shift to all loops of a given SCoP by using polyhedral operations⁴ that again affect the schedule *Sch*, see the δ^i terms in the $T(SZ, p, \delta)$ -formula in Sec. 2.

At this point there is only the *min*-operation left that keeps the HLS from generating unrolled parallel circuits for the innermost tile loop. There are two approaches to get rid of this. One option is to use index set splitting on the outer loop so that (a) all the full tiles have the same fixed number of iterations and can hence be unrolled, while (b) the incomplete last tile is cut off and processed separately. The consequences are not only a higher consumption of FPGA resources due to the duplication, but also a slower runtime

because the separate incomplete tile is unrolled less often which limits the overall throughput. We therefore pursue the other option: we round up the number of iterations in the last tile to the nearest integer multiple of the tile size, i.e., we pad the iteration space of the innermost tile loop, see Tiling 6 in Fig. 1. Note, that the extra iterations use hardware circuits that are already present, as full tiles also need them. The extra iterations do not cost runtime as the hardware circuits process them concurrently to the other iterations of the last tile. We implement the padding by modifying the domain *Dom* of the SCoP with polyhedral operations that take the lower and upper bounds plus the stride of the loop as well as the tile size into account and compute new upper bounds and a *mod*-operation that ensures that the resulting loop has the same stride as before.⁵ In the resulting Tiling 6 the inner tile loop always iterates 32 times, even if *i* reaches or surpasses *N*. As the buffers that are needed for the full tiles are sufficiently large to also hold the data that the padded last tile needs, there is no need for larger buffers.

Obviously we need countermeasures to prevent that the padded iterations change the semantics of the loop by writing to previously unused slots of the cache buffers or by working with uninitialized slots.

Let us talk about the two cases of write accesses first. (a) If the write access is not cached (**nc**), for example if it plays a role in a data dependence, we wrap it in a guarding *if* statement that keeps the extra iterations from writing. The branch statement hampers instruction level parallelism in the generated hardware, but as the HLS generates specific hardware, the negative effects are less severe than for a CPU's micro-instruction pipeline. (b) If the write access is cached, we trim the write back from the cache to the DDR accordingly, i.e., values in the cache buffer that are a result of padded iterations are not written back and hence do not affect the semantics of the loop. There is a corner case worth mentioning: assume the stencil would compute a value that is based on the number of iterations. It must store that value somewhere and modify it in every iteration. Hence, there is a write-after-write dependences which causes the above **nc**-case and thus the guards that switch off the effects of the added iterations. Hence, corner cases like this work correctly.

Whereas on CPUs computations with uninitialized values, e.g., a division by zero, may trigger exceptions that may give

³ $Sch' := Sch \cdot Adj$, where $Adj = tra(\Delta(tra(lmin(Sch(Dom))))^{-1})$. Note that *Sch* and *Dom* are of the ISL type union set and union map, resp. For the sake of simplicity we omit the space decomposition operator here. *tra* is ISL's translate operation.

⁴ $Sch' := Sch \cdot Zs$, where $Zs = \{O[ti_1, \dots, ti_d, i_1, \dots, i_d] \rightarrow O[ti_1, \dots, ti_d, p(i_1) - \delta_{p(ti_d)}^i, \dots, p(i_d) - \delta_{p(ti_d)}^i]\}$.

⁵For the SCoP's *Dom* let $S = stride(\downarrow_0(Dom))$ denote the stride of the innermost loop i_d and let $lb(Dom) = lmin(\downarrow_0(Dom))$ be the lower bound of this loop. Then $segStarts = \{S[i_1, \dots, i_d] \rightarrow S[i_1, \dots, \lfloor \frac{i_d - lb(Dom)}{SZ_d} \rfloor SZ_d + lb(Dom)]\}$ is the stream of index values at which the tiles start, i.e., the values of *ti*. From these starts we add SZ_d indices for each of the tiles, in particular for the last one. $padding = \{S[i_1, \dots, i_{d-1}, i_d] \rightarrow S[i_1, \dots, i_{d-1}, \pi] : i_d \leq \pi < i_d + SZ_d \wedge (\pi - i_d) \bmod S = 0\}$. In the resulting $Dom' := padding(segStarts(Dom))$ the *mod*-operations implement the stride of the original loop. For simplicity we omitted the permutation *p* from all the loop indices of the tile loops.

away the presence of padded iterations, FPGAs switch to NaN instead and thus hide the presence of the padding.

Step 4 – Index redirection Whenever we have assigned a buffer cache to an array access, the original array access needs to be retargeted to address the cache buffer instead of the original array. This is straightforward in case of full buffers, as it suffices to replace the name of the original array with the name of the cache buffer. All the index expressions in the code can remain unchanged. For chunk and line buffers however, we need to redirect the original index expressions. The new index expressions depend on the loop indices of the inter- and intra-tile loops, which in turn depend on the tiling transformation $T(SZ, p, \delta)$, and also on an offset relative to the upper left corner of the cache buffer. Let us skip the discussion of the lengthy and complex symbolic computations on the SCoP that make use of the polyhedral toolbox. Instead we refer both to a detailed discussion of a similar task in a PPCG-paper [31] and to the online data set and replication package [22] that accompanies this article.

To illustrate the index redirections at work, we consider the permutation (i, j, k) in Fig. 4. Instead of V we just access the full buffer V' which can be done with a simple text replacement in the SCoP of the loop nest. To retarget the stencil's two accesses to A to instead access the chunk buffer A' , we both replace $A[i, j, k]$ with $A'[0, j, k]$ and $A[i+1, j+1, k+1]$ with $A'[1, i+1, j+1]$. Here the first index expression of both redirected accesses no longer depends on the loop index i because the chunk buffer slice shifts by 1 whenever the i -loop ticks.

Step 5 – Code generation with declarations, pragmas, data shipment, halos, and bursts Here we generate code from the SCoP. For each of the buffer array, we add a static declaration just before the inner loops (inter-tile). The code in Fig. 5 shows this for the running example. For each buffer we also add a pragma `ARRAY_PARTITION` that tells the HLS to map the array to FPGA registers [37]. This prepares them for the concurrent accesses in the inner tile loop that the HLS unrolls/pipelines because of the added pragma `PIPELINE`. Note, that the HLS automatically duplicates parts of the buffer arrays to resolve access conflicts during pipelining. Hence, we do not need to add double buffering. But earlier works [1] manually added it to work around older HLS.

Data shipment. Depending on the type of buffer, we use different strategies to fill it before it is accessed. We initialize a *full* buffer completely before the first iteration of the tile and fully flush it after its last iteration. In Fig. 5 the first ship fills the buffer V' of the running example completely, i.e., it reads 1 (= last argument) single 3-dimensional (= next-to-last arg.) block of V starting from $V[ti, tj, tk]$. This reads what the upcoming tile (ti, tj, tk) needs. Let us postpone the discussion of the (pseudo-) macro `ship`.

```
// outer loops, inter-tile
for (ti=1;...) for (tj=1;...) for (tk=1;...) {
  float V'[32, 32, 32]; float A'[2, 33, 33];
  #pragma HLS ARRAY_PARTITION V' complete
  #pragma HLS ARRAY_PARTITION A' complete

  //fill V':
  ship(V,[ti,tj,tk],V',[0,0,0],3,1);
  // fill b1-1 2d-slices of A':
  ship(A,[ti,tj,tk],A',[0,0,0],2,1);
  for (i=0; i<=min(...); i++) {
    // fill b2-1 rows of A':
    ship(A,[ti+i+1,tj,tk],A',[1,0,0],1,1);
    for (j=0; j<=min(...); j++) {
      #pragma HLS PIPELINE
      // fill next row of A':
      ship(A,[ti+i+1,tj+j+1,tk],A',[1,j+1,0],1,1);
      for (k=0; k<32; k++) // padded loop
        V'[i,k,j] = V'[i,k,j] + A'[0,j,k]
          + A'[1,j+1,k+1];
    }
    // shift 1 slice of A' by 1:
    ship(A',[1,0,0],A',[0,0,0],2,1);
  }
  //flush V':
  ship(V',[0,0,0],V,[ti,tj,tk],3,1);
}
```

Figure 5. Generated code for the running example in Fig. 2 for $T(SZ=(32, 32, 32), p=(i, j, k), \delta=(-1, -ti_1, \dots, -1, -ti_d))$ with shared buffers $V'=[32,32,32]$, $A'=[2,33,33]$ from Fig. 4.

In their outermost dimensions the size a *chunk* array depends on the width of the bounding box of the index values that a tile computes. If an i -loop accesses $[i] \dots []$ and $[i+c] \dots []$, the width is $c+1$ and we pre-load c consecutive $d-1$ -dimensional data segments into the buffer before the tile starts. One level down in the intra-tile loops, the array's bounding box b_2 may be larger than the tile size SZ_2 . We then pre-load b_2-SZ_2 slices of $d-2$ -dimensional data. In general, the number of segments that a ship loads is the difference between the size of the bounding box and the tile size in the corresponding dimension.

In Fig. 5, there are three ship operations that fill the chunk buffer A' before the tile's body runs. The first ship loads one (= last arg.) 2-dimensional chunk (= next-to-last arg.) of data to the buffer, as the bounding box has size $c=2$ in the most significant dimension. Afterwards one 2-dimensional slice with sizes $[1, 33, 33]$ remains to be loaded. Since in the next dimension down the intra-tile loops, we have $b_2=33$ and $SZ_2 = 32$, the second ship fills a line of A' . Both the line with the i -loop and the index in the source array A tick. Just before the innermost loop we ship the remaining line into A' . Its indices into A move with both the i - and the j -loop. After the three data shipments the chunk buffer is complete and the tile body can run. Then a ship shifts the data within the chunk buffer so that some data (needed by later sub-tiles) remain in the buffer, albeit at a different index; the shift also makes room to (pre-)load new data for the next sub-tile.

```

// src, src-offset, dest, dest-offset
// di dimensional segment, R repetitions
ship(S, [osd, ..., osdi+1, osd, ..., os1],
      D, [odd, ..., oddi+1, odd, ..., od1], di, R);

for (r=0; r<R; r++)
  for (sdi=0; sdi < DSdi; sdi++)
    ...
      for (s2=0; s2 < DS2; s2++)
        burstcpy(D[odd, ..., oddi+1, odd + sdi + ci, ..., od1 + s1],
                  S[osd, ..., osdi+1, osd + sdi + ci, ..., os1 + s1], DS1);

```

Figure 6. The semantics of the ship macro.

Halos and bursts. The ship (pseudo-) macro expands into a nest of loops, one per array dimension, see Fig. 6. The additional enclosing loop deals with the number of repetitions if, as in case of the initial ship of the chunk buffer A', a few segments need to be copied. The innermost array dimension is copied in memcpy-style (instead of another loop that would copy values one element at a time).

If we actually used memcpy, the HLS would generate standard DMA operations that, in general, process one array value per cycle of the FPGA hardware. Luckily, by specifying a so-called *port width* w we can direct the HLS to generate a channel of width w that handles w values per cycle. This bursts the filling and flushing of buffers by a factor of w and significantly improves performance, see Sec. 6. However, there is a downside: Bursts require that both the DDR-side memory address and the number of array elements to be shipped are divisible by w .

To exploit the bursting ability we thus need to extend buffers with slightly larger ones, more specifically, we round up the size of the innermost array dimension to the next size that is divisible by w . In the example, for $w=4$ we actually declare and allocate an array A'' of size [2,33,36] that is large enough to host the buffer A' with halo elements around it. But how many of the 3 halo elements in the last dimension live on which side of the buffer A'? To answer this question we need to look at the first element of the original array A that needs to be copied into the buffer. If this array element is not aligned w.r.t. to the w -addressing requirements, we need to copy a few more values left of it. The number of extra values determines how many halo elements A'' needs to have on the left of the buffer A'.⁶

5 Related Work

Our work is related to a range of different publications. Many works use polyhedral methods for reuse detection in a software environment. Many approaches [4, 17, 24, 25, 36]

⁶In our implementation, step 2 of course works with the sizes of the halo-added buffers. And the index redirections in step 4 take the number of halo elements into account and compute replacement indices that are displaced by the number of needed halo elements. And finally, the code generator earlier in step 5 declares buffer arrays with halos and uses ship operations that use the displaced indices. We hid the index displacements so far as they would have affected the digestibility of the explanations through the paper.

reorder memory accesses to benefit from the multilayer-multipurpose caches present on modern CPUs and some [24, 25] also employ explicit multi-buffering to scratch-pads, but these concepts cannot easily be transferred to standard FPGA architectures that are not equipped with such caches or scratch-pads. PPCG [31] is a source-to-source compiler that uses the polyhedral model to generate SIMD parallelism for a GPU. Despite generating CUDA code instead of HLS C the approach is similar to ours as it uses temporary arrays to buffer reused data. It does not address aspects like bursts or pipeline performance, as these are unique to hardware design. The method is evaluated on ten benchmarks from the PolyBench collection, including the 6 stencil codes that we also look at. They do not evaluate on the Adept benchmark from our set. Dtg_codegen [33] generates SIMD instructions for machine learning codes. Similar to our step 3, it adds padding iterations when the iteration space cannot be tiled evenly, but it does not address burst or pipeline performance. The model from Van Achteren et al. [29] calculates from loop nests how to best exploit scratch-pad memories, but it does not employ multiple buffer types, does not optimize the data shipment, and does not use loop tiling.

Some authors [6, 7, 20, 35] add multipurpose caches to FPGA architectures to exploit data reuse and to speed up performance. This approach typically does not require any complex analysis of the input code and therefore does not utilize polyhedral methods. In turn, the heuristics of multipurpose caches limit the performance gain and also severely limit the possibilities for bus widening. However, our technique is limited to homogeneous and statically determined reuse patterns, whereas multipurpose caches have no such limitation. Since we can detect array accesses that we cannot cache (**nc**-label), combining our approach with a multipurpose cache for such accesses may be beneficial. All four works ignore established benchmark sets and evaluate only on small, proprietary sets of eight or fewer benchmarks.

Liu et al. [19] utilize polyhedral methods in an FPGA environment. Their approach uses polyhedral analysis to perform loop splitting and thereby increases the loop pipelining performance. In contrast, our goal is to increase the effective storage throughput, and we therefore generate vastly different hardware. They only present quantitative results for one stencil code (2d jacobi) and achieve small speedups (2.7) compared to our 17 – 39 on the same 2d jacobi kernel, probably because they do not use any buffers. On the other hand, their approach is not limited to stencil code and could therefore be used to speed up loops where our method is inapplicable.

Friebe et al. [15] translate fluid dynamic tensors from a DSL to HLS C. They use the polyhedral model to find dependences and reschedule operations to reduce their distances. This optimization is potentially orthogonal to ours, but does not employ any reuse or burst optimizations.

Closer related to us are works that generate FIFO channels to buffer reusable data [8, 23, 26, 34]. These works, like ours,

use polyhedral methods in the FPGA domain to improve on data reuse. However, their approach to hardware generation is significantly different from ours. Instead of building cache structures, they use the polyhedral method to split the stencil code into multiple hardware blocks and connect them via FIFO channels through which reusable data is sent to the next consumer. The method promises a smaller resource utilization than ours but cannot be fully implemented on HLS source level, and therefore cannot utilize modern, highly optimized HLS tools. It also does not allow for any burst optimizations and bus widening. Since in contrast to us, the AutoSA research tool [34] can handle non-canonical loop nests, we cannot evaluate their benchmark codes in our systems. While it would be interesting to study and compare the FPGAs that AutoSA generates from our stencil codes, we could not upgrade their system from the older Vitis HLS 2019.2 that they used to the current one. The numbers in the papers cannot be compared because of the different optimizations that the HLS versions provide. Meeus et al. [23] and Natale et al. [26] evaluate only about half the stencils we look at. They mainly focus on resource or energy efficiency instead of runtime performance. Cong et al. [8] and Wang et al. [34] do not show any results on stencil codes.

Issenin et al. [13] use polyhedral methods to improve data-reuse on ASICs by employing scratch-pad RAM. As the work is not focused on a specific problem area, it has to rely on highly complex models that on larger codes require extreme runtimes. (In practice, the user can cut the optimization short but has to accept sub-optimal results.) The publication therefore evaluates the performance with only four algorithm snippets, all from the field of computer graphics. We use a much broader set of stencils in our evaluation.

Pouchet et al. [28] propose a framework for optimizing stencil codes. One of its features is a polyhedral-based data-reuse optimization similar to ours. However, they only cover cases where reuse occurs between two consecutive iterations of the innermost stencil loop. Our work has none of these limitations. Their method is inapplicable to about half of our benchmarks set. For most of the remaining stencils their restrictions lead to many more memory accesses than our method (3x for 2D-5P).

Deeus et al. [9] and Alias et al. [1] both present FPGA code generators that use tiling to exploit intra-tile *and* inter-tile data reuse. While our approach can be orthogonally extended with their inter-tile reuse method, our intra-tile reuse method is more advanced as it defines three buffer types, picks them depending on the tiling permutation, and is unique in using wide bursts to increase the bandwidth.

6 Evaluation

To evaluate we use all 4 stencil codes from the Adept benchmark suite [14] and 4 (out of 6) stencil codes from PolyBench [27]. We exclude *adi* as it uses a non-canonical loop nest.

Table 1. Characteristics of the Benchmark Set.

name	dimen- sions	stencil points	shared buffers	in- place	F_{max} in MHz
1D-jacobi	1	4	2	no	124
2D-5p	2	5	2	no	261
2D-9p	2	9	2	no	205
2D-jacobi	2	6	2	no	200
2D-fdtd0	2	4	2	yes	345
2D-fdtd1	2	4	2	yes	320
2D-fdtd2	2	6	3	yes	260
3D-19p	3	19	2	no	145
3D-27p	3	27	2	no	55
3D-heat	3	11	2	no	50

The data dependences in *seidel* prevent loop tiling. Since in *fdtd* there are three distinct sub-stencils that we evaluate separately, we have a set of 10 codes. Table 1 holds some relevant characteristics. The set has a range from simple 4-point stencils up to a 27-point stencil. Note that there is a lot of data-reuse. Step 2 of Sec. 4 can always fuse the accesses into 2 or 3 shared buffers. Except for the *fdtd*-benchmarks that update their arrays in place, all codes use shadow arrays to compute new values and hence do not have any (loop-independent) dependences.

We use the OpenMP-to-FPGA compiler ORKA-HPC [21] to offload code fragments to the FPGA that are flagged with the target pragma. Our Ubuntu 20.04.4 LTS test system with an Intel Core i7-4770 CPU is connected to a Xilinx VCU118 FPGA board via PCI express (width x4, 5GT/s). We synthesize the FPGA hardware with Xilinx Vitis 2021.2. TaPaSCo DSE [18] finds the highest possible frequencies (F_{max} in Table 1) for the hardware synthesis of the codes. But to ease comparison, we always used 50 MHz to measure the speedups (even though higher frequencies would yield higher speedups). To derive SCoPs from the canonical loop nests of the stencils we rely on the Polyhedral Extraction Tool (PET) [32].

For each benchmark, we measure and average the runtimes of 5 runs, excluding the time it takes to initially ship the data from the host to the DDR memory on the FPGA board. Below we discuss the speedups that our optimized FPGAs achieve in comparison to the baseline, i.e., the FPGA that the HLS generates with its default settings. The baseline does not use any buffering (and there is no burst-enhanced data shipment), but there is an implicit PIPELINE pragma in the innermost stencil loops. We use fixed seeds to generate the same random input arrays (with 64 MiB of data) for all measurements. All FPGA versions have the same results as a sequential run of the stencil on the CPU.

Impact of the tile sizes. For all 10 benchmarks (ordered by data dimensionality), Fig. 7 shows the speedups over the baseline for large tile sizes with 3-5 hours of HLS time. Halving the sizes in each dimension (= small tiles) causes the speedup to drop significantly, by a factor of 1.3x to 2.5x. Larger tiles are better because of two main reasons. First,

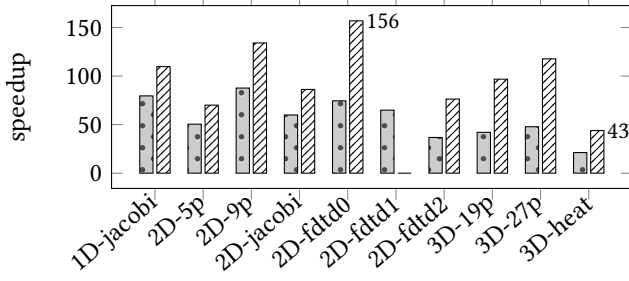


Figure 7. Speedups of two optimized FPGAs for varying tile sizes (and port widths 16). Small Tiles \square : $SZ_{1D}=(512)$, $SZ_{2D}=(64, 64)$, $SZ_{3D}=(16, 16, 16)$. Large Tiles \square : $SZ_{1D}=(1024)$, $SZ_{2D}=(128, 128)$, $SZ_{3D}=(32, 32, 32)$. Empty bar: HLS failed with a timing error.

larger tile sizes lead to more parallel hardware as the HLS can unroll larger innermost intra-tile loops. Second, the unrolled basic blocks lead to bigger/deeper pipelines that can better hide memory latencies. Theoretically this can explain a factor of $2\times$. The range we see in the numbers is caused by both the number/sizes of the cache buffers and the amount of reuse. The data must be loaded into the buffers before the tiles access it. For full buffers the HLS cannot overlap the filling of the buffers and the execution of a tile, as the data needs to be in the buffer before it is accessed. For chunk buffers we carefully crafted the pre-loading of segments of the data so that the HLS can partly overlap the loading with ship operations further down the tile’s loop nest. For full buffers and, because of the pre-loading, even for chunk buffers, each load has a fixed runtime overhead. The more often the tile uses a data in the buffer, the better it can amortize these fixed costs. This explains why we see factors around $2\times$ for the high-point stencils. The low-point stencils have factors around $1.3\times$. (2D-9p and 3D-heat are mid-tier.) The exception to the rule are the fdt stencils. Despite being 4-point stencils they strongly benefit from larger tile sizes. The reason is their in-place updates. Whereas our optimized FPGAs can map them to fast register operations, the baseline FPGA always keeps them sequential.

Impact of the port width. Fig. 8 shows that wider bursts boost performance as they increase memory throughput and fill buffers faster. Note, that the second bar of each benchmark is the same as in Fig. 7. As mentioned before, even though HLS can sometimes partly overlap the filling of the buffers with the unrolled/pipelined tile, there are still fixed costs. Hence, a quicker buffer initialization has a direct impact on the overall runtime performance. The smaller the runtime of a tile is, the harder it is for the tile to amortize the fixed costs, and hence the more impact an increased port width has. The impact of the port width is stronger whenever the impact of the tile size is smaller, and the other way round.

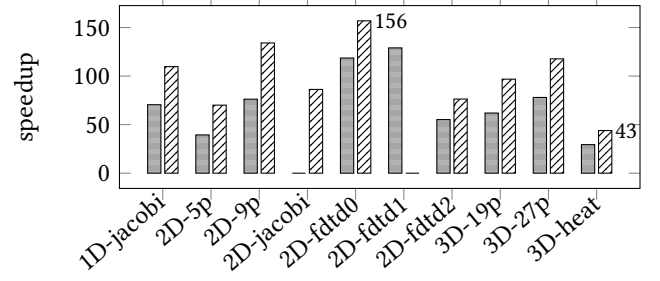


Figure 8. Speedups of two optimized FPGAs for port widths 8 \square and 16 \square (and large tile sizes $SZ_{1D}=(1024)$, $SZ_{2D}=(128, 128)$, $SZ_{3D}=(32, 32, 32)$). Empty bar: as before.

This is exactly what a comparison of Fig. 7 and Fig. 8 reveals.

We do not show bars for the combination of two bad choices, i.e., for small tile sizes and a small burst width, since this leads to an even stronger drop of the achieved speedups.

Importance of the right permutation and of padded tile loops. Let us now demonstrate that some of the choices in Sec. 4 are crucial for the performance. Instead of working with all benchmark codes we pick 2D-5p as it is affected the least by bad choices. For the other benchmarks the effect of a wrong choice is even stronger. We do not consider the three fdt codes because of their irregular in-place behavior. And we also ignore the stencils for which the HLS refuses to generate an FPGA. The 5-point stencil 2D-5p is computationally the most simple one in the remaining set.

In Sec. 4, step 2 picks the permutation that needs the smallest total buffer size. For the 10 stencils, it considers 1–6 potential permutations. For each benchmark there are two groups of permutations. The more costly group requires 2 or 3 full buffers whereas the cheaper group can do without any full buffers. For the total runtime of a stencil on the FPGA, we need to look at the sum of the buffer filling time and the tile’s execution time, it is the number and the size of the full buffers that make the selection of a wrong permutation most obvious. Compared to 3D stencils, 2D stencils like 2D-5p are less affected by a wrong choice of buffer type as their full buffers are smaller (as they only need to store 2D data).

For 2D-5p we saw in Fig. 7 a speedup of $70\times$ over the baseline. For this speedup, step 2 picked a chunk buffer and a line buffer. When picking a wrong permutation instead, we see a smaller speedup. The achieved speedup of the generated FPGA drops from $70\times$ down to $21\times$. Picking the best permutation is even more important for computationally more demanding stencils with larger working sets.

Step 3 of Sec. 4 removed the min-operation from the innermost loop. This caused the last tile to always be a full one. The rationale that this enables the HLS to unroll/pipeline the innermost loop is justified in the 10 benchmarks. For code versions that still have the min-operations the HLS generates

sequential hardware for the innermost loop; the bodies are no longer executed in parallel. (The HLS protocols reveal that there is no unrolling and the consumption of DSP blocks shrinks by $8\times$ – $22\times$ which indicates sequential behavior.)

When we switch off the padding of the innermost tile loop of 2D-5p, there is not just a reduced speedup. The resulting FPGA is even *slower* than the baseline FPGA by a factor of $2\times$ (whereas the padded version saw a speedup of $70\times$). Loop padding is even more important for computationally more demanding stencils.

7 Conclusion

This paper presents an optimization that offloads memory-bound stencil codes to FPGAs that are $43\times$ and $156\times$ faster than the hardware that the HLS generates with its default optimization settings. The presented technique uses polyhedral methods to pick the best loop tiling that – when inlined cache buffers are added to exploit data-reuse – achieves the best runtime. Other key insights are that the iteration space of the intra-tile loops should be padded to avoid incomplete tiles, that heavy tiling of the iteration space enables the HLS to unroll/pipeline the tiles into concurrent hardware, and that by adding halo elements to the cache buffers and properly aligning the memcopy operations, the HLS can utilize wide bursts to further boost the runtime performance.

References

- [1] Christophe Alias, Alain Darte, and Alexandru Plesco. 2013. Optimizing remote accesses for offloaded kernels: Application to high-level synthesis for FPGA. In *Proc. Intl. Conf. on Design, Automation and Test in Europe (DATE'13)*. Grenoble, France, 575–580.
- [2] Jason Ansel, Shoaib Kamil, Kalyan Veeramachaneni, Jonathan Ragan-Kelley, Jeffrey Bosboom, Una-May O'Reilly, and Saman Amarasinghe. 2014. OpenTuner: An extensible framework for program autotuning. In *Proc. Intl. Conf. on Parallel Architecture and Compilation Techniques (PACT'14)*. Edmonton, Canada, 303–315.
- [3] Mohamed-Walid Benabderrahmane, Louis-Noël Pouchet, Albert Cohen, and Cédric Bastoul. 2010. The Polyhedral Model Is More Widely Applicable Than You Think. In *Proc. Intl. Conf. on Compiler Construction (CC'10)*. Paphos, Cyprus, 283–303.
- [4] Uday Bondhugula, Albert Hartono, J. Ramanujam, and P. Sadayappan. 2008. A Practical Automatic Polyhedral Parallelizer and Locality Optimizer. In *Proc Intl. Conf. on Programming Language Design and Implementation (PLDI'08)*. Tucson, AZ, 101–113.
- [5] Pierre Boulet, Alain Darte, Georges-André Silber, and Frédéric Vivien. 1998. Loop Parallelization Algorithms: From Parallelism Extraction to Code Generation. *Parallel Comput.* 24, 3–4, Article 5 (May 1998), 24 pages.
- [6] Julian Brandner, Florian Mayer, and Michael Philippsen. 2023. Multi-purpose Cacheing to Accelerate OpenMP Target Regions on FPGAs. In *Proc. Intl. Conf. on OpenMP (IWOMP'23)*. Bristol, UK, 147–162.
- [7] Brignone, Giovanni and Usman Jamal, M. and Lazarescu, Mihai T. and Lavagno, Luciano. 2022. Array-Specific Dataflow Caches for High-Level Synthesis of Memory-Intensive Algorithms on FPGAs. *IEEE Access* 10 (2022), 118858–118877.
- [8] Jason Cong, Muhuan Huang, Peichen Pan, Yuxin Wang, and Peng Zhang. 2016. Source-to-Source Optimization for HLS. In *FPGAs for Software Programmers*, Dirk Koch, Frank Hanning, and Daniel Ziener (Eds.). Springer International Publishing, Basel, Switzerland, Chapter 8, 137–163.
- [9] Gaël Deest, Nicolas Estibals, Tomofumi Yuki, Steven Derrien, and Sanjay Rajopadhye. 2016. Towards Scalable and Efficient FPGA Stencil Accelerators. In *Proc. Intl. Workshop Polyhedral Compilation Techniques (IMPACT'16)*. Prague, Czech Republic.
- [10] Paul Feautrier. 1992. Some efficient solutions to the affine scheduling problem. I. One-dimensional time. *Intl. Journal of Parallel Programming* 21, 5 (Oct. 1992), 313–347.
- [11] Björn Franke and Michael O'Boyle. 2003. Array Recovery and High-Level Transformations for DSP Applications. *ACM Trans. Embedded Computing Systems* 2, 2 (May 2003), 132–162.
- [12] Tobias Grosser, Sven Verdoolaege, and Albert Cohen. 2015. Polyhedral AST Generation Is More Than Scanning Polyhedra. *ACM Trans. Program. Lang. Syst.* 37, 4, Article 12 (July 2015), 50 pages.
- [13] Ilya Issenin, Erik Brockmeyer, Miguel Miranda, and Nikil Dutt. 2007. DRDU: A Data Reuse Analysis Technique for Efficient Scratch-Pad Memory Management. *ACM Trans. Design Automation of Electronic Systems* 12, 2, Article 15 (Apr. 2007), 28 pages.
- [14] Nick Johnson. 2015. The Adept Benchmark Suite. Retrieved November 10, 2023 from <https://github.com/EPCCed/adept-kernel-openmp>
- [15] F. A. Karl Friebe, Stephanie Soldavini, Gerald Hempel, Christian Pilato, and Jeronimo Castrillon. 2021. From Domain-Specific Languages to Memory-Optimized Accelerators for Fluid Dynamics. In *Intl. Conf. on Cluster Computing (CLUSTER'21)*. Portland, OR, 759–766.
- [16] Richard M. Karp, Raymond E. Miller, and Shmuel Winograd. 1967. The Organization of Computations for Uniform Recurrence Equations. *J. ACM* 14, 3, Article 12 (July 1967), 28 pages.
- [17] Induprakash Kodukula, Nawaaz Ahmed, and Keshav Pingali. 1997. Data-Centric Multi-Level Blocking. In *Proc. Intl. Conf. on Programming Language Design and Implementation (PLDI'97)*. Las Vegas, NV, 346–357.
- [18] Jens Korinth, Jaco Hofmann, Carsten Heinz, and Andreas Koch. 2019. The TaPaCo Open-Source Toolflow for the Automated Composition of Task-Based Parallel Reconfigurable Computing Systems. In *Proc. Intl. Symp. on Applied Reconfigurable Computing (ARC'19)*. Darmstadt, Germany, 214–229.
- [19] Junyi Liu, John Wickerson, and George A. Constantinides. 2016. Loop Splitting for Efficient Pipelining in High-Level Synthesis. In *Proc. Intl. Symp. on Field-Programmable Custom Computing Machines (FCCM'16)*. Washington, DC, 72–79.
- [20] Liang Ma, Luciano Lavagno, Mihai Teodor Lazarescu, and Arslan Arif. 2017. Acceleration by Inline Cache for Memory-Intensive Algorithms on FPGA via High-Level Synthesis. *IEEE Access* 5 (2017), 18953–18974.
- [21] Florian Mayer, Julian Brandner, Matthias Hellmann, Jesko Schwarzer, and Michael Philippsen. 2021. The ORKA-HPC Compiler—Practical OpenMP for FPGAs. In *Proc. Intl. Workshop Languages and Compilers for Parallel Computing (LPCP'21)*. Newark, DE, 83–97.
- [22] Florian Mayer, Julian Brandner, and Michael Philippsen. 2023. Replication Package for “Employing polyhedral methods to optimize stencils on FPGAs with stencil-specific caches, data reuse, and wide data bursts”. <https://doi.org/10.5281/zenodo.10396084>
- [23] Wim Meeus and Dirk Stroobandt. 2018. Data Reuse Buffer Synthesis Using the Polyhedral Model. *IEEE Trans. Very Large Scale Integration (VLSI) Systems* 26, 7, Article 12 (July 2018), pp. 1340–1353 pages.
- [24] Benoît Meister, Allen Leung, Nicolas Vasilache, David Wohlford, Cédric Bastoul, and Richard Lethin. 2009. Productivity via Automatic Code Generation for PGAS Platforms with the R-Stream Compiler. In *Proc. Intl. Workshop Asynchrony in the PGAS Programming Model (APGAS'09)*. Yorktown Heights, NY.
- [25] Benoît Meister, Nicolas Vasilache, David Wohlford, Muthu Manikandan Baskaran, Allen Leung, and Richard Lethin. 2011. R-Stream Compiler. In *Encyclopedia of Parallel Computing*, David A. Padua (Ed.). Springer US, 1756–1765.

- [26] Giuseppe Natale, Giulio Stramondo, Pietro Bressana, Riccardo Cattaneo, Donatella Sciuto, and Marco D. Santambrogio. 2016. A polyhedral model-based framework for dataflow implementation on FPGA devices of Iterative Stencil Loops. In *Proc. Intl. Conf. on Computer-Aided Design (ICCAD'16)*. Austin, TX, 1–8.
- [27] Louis-Noël Pouchet. 2015. PolyBench/C – The Polyhedral Benchmark Suite. Retrieved November 10, 2023 from <http://web.cse.ohio-state.edu/~pouchet.2/software/polybench/>
- [28] Louis-Noël Pouchet, Peng Zhang, P. Sadayappan, and Jason Cong. 2013. Polyhedral-Based Data Reuse Optimization for Configurable Computing. In *Proc. Intl. Symp. on Field Programmable Gate Arrays (FPGA'13)*. Monterey, CA, 29–38.
- [29] Tanja Van Achteren, Geert Deconinck, Francky Catthoor, and Rudy Lauwereins. 2002. Data Reuse Exploration Techniques for Loop-Dominated Applications. In *Proc. Intl. Conf. on Design, Automation and Test in Europe (DATE'02)*. Valencia, Spain, 428–435.
- [30] Sven Verdoolaege. 2010. ISL: An Integer Set Library for the Polyhedral Model. In *Proc. Intl. Congress on Mathematical Software (ICMS'10)*. Kobe, Japan, 299–302.
- [31] Sven Verdoolaege, Juan Carlos Juega, Albert Cohen, José Ignacio Gómez, Christian Tenllado, and Francky Catthoor. 2013. Polyhedral Parallel Code Generation for CUDA. *ACM Trans. Architecture and Code Optimization* 9, 4, Article 54 (Jan 2013), 23 pages.
- [32] Sven Verdoolaege and Tobias Grosser. 2012. Polyhedral Extraction Tool. In *Proc. Intl. Workshop Polyhedral Compilation Techniques (IMPACT'12)*. Paris, France.
- [33] Sven Verdoolaege, Manjunath Kudlur, Robert S. Schreiber, and Harinath Kamepalli. 2020. Generating SIMD Instructions for Cerebras CS-1 using Polyhedral Compilation Techniques. In *Proc. Intl. Workshop Polyhedral Compilation Techniques (IMPACT'20)*. Bologna, Italy.
- [34] Jie Wang, Licheng Guo, and Jason Cong. 2021. AutoSA: A Polyhedral Compiler for High-Performance Systolic Arrays on FPGA. In *Proc. Intl. Symp. on Field-Programmable Gate Arrays (FPGA'21)*. Virtual Event, 93–104.
- [35] Felix Winterstein, Kermin Fleming, Hsin-Jung Yang, John Wickerson, and George Constantinides. 2015. Custom-sized caches in application-specific memory hierarchies. In *Proc. Intl. Conf. on Field Programmable Technology (FPT'15)*. Queenstown, New Zealand, 144–151.
- [36] Michael E. Wolf and Monica S. Lam. 1991. A Data Locality Optimizing Algorithm. In *Proc. Intl. Conf. on Programming Language Design and Implementation (PLDI'91)*. Toronto, Canada, 30–44.
- [37] Xilinx. 2023. Vitis High-Level Synthesis User Manual. Retrieved November 10, 2023 from <https://docs.xilinx.com/r/en-US/ug1399-vitis-hls>